PAPER 28 (SESSION II)

# Motion of cracks in brittle fracture

Prof. J. DVORAK
Duke University, Durham, North Carolina, U.S.A.

**Summary**

Some features of the micromechanism of crack propagation in steel and similar metals are discussed and a model for the description of crack motion is proposed and analyzed.

Two modes of material separation exist at the tip of a running brittle crack. Easy cleavage or, propagation of cleavage microcracks which results in formation of a continuous, multiply connected, nearly planar path with a highly irregular front which spreads both forward and laterally through favorably oriented grains ahead of the crack tip. The remaining material forms disconnected links which span the prospective fracture surface behind the easy cleavage front. Plastic deformation which precedes fracture of the links, accounts for the major part of energy dissipated in fracture propagation.

While the main crack propagates, bursts of easy cleavage spread ahead, become arrested and reinitiated. This periodic process leads to stepwise propagation of the cleavage crack front and to velocity variation at the tip of the main crack.

The kinematics of crack motion is investigated quantitatively for the case of a steady state crack in plane strain. The influence of applied load, material properties and grain size upon crack motion is described. It is shown that two different modes of stepwise motion are possible, depending on grain size and crack velocity. The calculated values of step length are in good agreement with available experimental measurements.

## Introduction

This paper presents a continuum analysis of the kinematics of motion of the tip of a running brittle crack. It is based on a recent study of the micromechanism of material separation in brittle fracture [1].

The important feature of steel and similar b.c.c. metals is their ability to deform and fracture in two different modes. At low strain rates and at higher temperatures, the general behavior is characterized by slip and rupture and by a pronounced sensitivity to variation of the two parameters. When the rate of straining is sufficiently high or when the temperature decreases, a gradual transition to deformation by twinning and to separation by cleavage is observed. Those are essentially rate insensitive processes, but within individual grains they are limited to certain crystallographic directions and planes so that on the microscale, grain orientation becomes important. In particular, cleavage microcracks may form at the first few twins and propagate through favorably oriented grains, while the bulk of the material is still elastic [2-4].

At the high strain rates which exist in the vicinity of the tip of a running brittle crack, twinning and cleavage are dominant in a wide

temperature range below the transition value which is found in most steels at ambient temperatures. When the transition phenomena, such as energy or fracture mode transitions are excluded, it can be shown that two basic modes of material separation exist at the tip of a running brittle fracture. Easy cleavage or, propagation of microcracks through favorably oriented grains, forms a continuous, very irregular multiply connected but nearly planar path involving at least one half of the grains and leaves behind disconnected links consisting of grains of less favorable orientations which span the prospective fracture surface. This is indeed frequently observed in arrested cracks, Fig. 1. An idealized view of such crack zone is shown in Fig. 2 for the case of uniform weakening which will be assumed here. The remaining links deform plastically, mainly by twinning and when the crack opening displacement in the crack zone increases sufficiently, they finally cleave. The mechanical properties of the links, as derived in [1] are shown in Figs. 3 and 4, respectively. The stress $\sigma_P$ is the limit load of the links, $\epsilon_c$ is their fracture strain and $\sigma_0$ is the minimum stress, normal to the fracture surface, which will maintain propagation of easy cleavage microcracks. The latter depends both on grain size $d$ and on the surface energy $\gamma$. The stress $\sigma_c$ is the twinning cleavage stress and it may be considered as the yield stress of the material in the vicinity of the crack zone. Since $\sigma_P$ is close to $\sigma_c$, the plastic straining at the crack tip will be limited only to the links or, to a thin layer at the fracture surface and will not extend into the surrounding matrix. Hence, easy cleavage is instrumental in determination of the shape of the plastic zone at a running brittle crack.

Deformation and fracture of the links will control the energy balance of the propagation process. While in brittle materials, the crack speed is independent of the applied load and assumes always its limiting value, an equilibrium velocity, which depends on load is observed in ductile materials, like plastics and steel [5-9]. This indicates that the rate of energy dissipation in the fracture process increases with crack speed, Fig. 5. Such consideration applies to the speed of separation of the links, since the energy required for easy cleavage is very small. The velocity of motion of the easy cleavage front does not depend on the applied load but on other parameters and, for the conditions present at the tip of a running brittle crack, it has been estimated as a constant fraction of the shear wave velocity, $V_C = 0{\cdot}6\ c_2$ [1]. On the other hand, the experimentally observed variation of brittle fracture speed in steel extends from a minimum at about $0{\cdot}05\ c_2$, which is clearly implied by the requirement of high strain rate at the crack tip, to a limiting speed, $0{\cdot}6\ c_2$ [7, 10]. Therefore, the two separation modes will proceed at two different velocities and a stepwise motion of the crack will result.





**Motion of the crack zone**

Let us consider that a steady state crack propagates under plane strain conditions in a steel plate. Since the approximate shape of and the stresses transmitted in the crack zone are known, the stress field in the vicinity of the crack tip can be found from an elastic solution. Although the present model predicts some variation in crack speed, steady state solutions will be still used as approximations for analysis of stresses and displacements. The particular crack configuration considered here was originally proposed by Craggs [11], Fig. 6. When an uniaxial compression $\sigma_{yy} = -P$ is superimposed, all external loads will be reduced to the crack line, Fig. 7.

The individual events in motion of the crack zone are indicated in Fig. 7. At $t = t_0$, the plastic deformation spreads through the entire zone, up to the arrested cleavage front, Fig. 2. This front is very irregular, the links at this location are a part of the unfractured material ahead of the zone. When twinning occurs there, new microcracks will form and initiate a new step of easy cleavage. The tip $C$ of the crack zone rapidly attains the limiting velocity of easy cleavage, $V_C$. The velocity of the main crack is $V_A = V_1 < V_C$. At time $t = t_p$, the cleavage front enters a location ahead of the original zone where $\sigma_{yy} = \sigma_0$ and becomes arrested, Fig. 7 (b). The velocity of point $A$ increases to $V_A = V_2 > V_1$. Both points $A$ and $B$ will move towards $C$ and when the entire zone becomes plastic, another step of easy cleavage will commence.

A schematic representation of motion of individual points of the crack zone is shown in Fig. 8. Two different modes of motion are possible. When the penetration time $t_p$ is short, the stress field at point $C$ will be determined by the crack zone speed which existed at $t = t_0$, Fig. 7 (a). Indeed, as cleavage spreads ahead, the crack opening displacement in the zone will gradually increase. This effect will be felt at point $A$ at time $t = t_1$. Since the strain at the crack tip $A$ must not exceed the critical value $\epsilon_c$, the velocity of $A$ will increase. However, this will not be transmitted to point $C$ until $t = t_2$. Therefore as long as $t_p < t_2$, there will be no interference of crack tip acceleration with motion of the cleavage front. On the other hand, when the penetration time becomes sufficiently long, $t_p > t_2$, the stress field at the cleavage front $C$ will be affected by the acceleration and the length of the penetration step will increase accordingly. These two modes of crack zone motion will be analyzed separately.

The arrest of the cleavage front $C$ at time $t = t_p$ will be felt at point $A$ at $t = t_4$. The velocity $V_A$ will again decrease to $V_A = V_1$ and, at $t = t_5$, the crack zone will assume the fully plastic configuration.

While it is expected that the main crack tip velocity $V_A$ will change continuously, it will be approximated, as indicated in Fig. 8, by two constant average velocities $V_1$ and $V_2$ in the respective time intervals.

**Motion without interference**, $t_p < t_2$

Consider an elastic semi-infinite crack with an arbitrary crack opening load $f(-x)$ applied within $-a < x < 0$ on the crack line. Then, the distribution of the stress normal to the positive $x$ axis will be, at any constant crack velocity $V$, [11, 12]

$$\sigma_{yy}(x)_{|y=0} = -\frac{1}{\pi}\left\{\mathrm{Im}\int_{-\sqrt{a}}^{\sqrt{a}} \frac{f(t^2)\,dt}{t - i\sqrt{x}} - \frac{1}{\sqrt{x}}\int_0^a \frac{f(t)\,dt}{\sqrt{t}}\right\} \tag{2}$$

The crack opening displacement on the negative $x$ axis,

$$v(-x)_{|y=0} = B(V)\int_{\sqrt{a}}^{\sqrt{a}} f(t^2)\,[\zeta + t\,\lg|t-\zeta|]\,dt \tag{3}$$

and $\zeta = -\sqrt{-x}$.

Where appropriate, the principal value of the integrals in equations (2) and (3) must be taken. The velocity function $B(V)$ in equation (3) is given for the case of plane strain as:

$$B(V) = \frac{2\dfrac{V^2}{c_2^2}\left(1-\dfrac{V^2}{c_1^2}\right)^{1/2}}{\pi\mu\left[4\left(1-\dfrac{V^2}{c_1^2}\right)^{1/2}\left(1-\dfrac{V^2}{c_2^2}\right)^{1/2} - \left(2-\dfrac{V^2}{c_2^2}\right)^2\right]} \tag{4}$$

$$c_1^2 = \frac{\lambda + 2\mu}{\rho}, \quad c_2^2 = \frac{\mu}{\rho}$$

where $\lambda$, $\mu$ are Lame's elastic constants and $\rho$ is the density.

The analysis of the initial crack configuration, Fig. 7 (a), can now be made. The length $s_0$ of the fully plastic crack zone is found from the condition that stresses must be finite at point $C$. The familiar finiteness conditions is

$$P\sqrt{(a)} - \sigma_P\sqrt{(s_0)} = 0. \tag{5}$$

Then, from equation (3),

$$v_A = B(V_1)\frac{P^2 a}{\sigma_P}. \tag{6}$$

However, by definition

$$v_A = \epsilon_c\,\Delta(V_1) \tag{7}$$





where $\Delta(V_1)$, which is a function of velocity, represents the thickness of the plastically deformed layer at the fracture surface. From equations (6) and (7),

$$P^2 a = \sigma_P \epsilon_c \frac{\Delta(V_1)}{B(V_1)}. \tag{8}$$

This relation implies that the loading factor $P\sqrt{a}$ will increase with velocity if

$$\frac{\partial}{\partial V}\left[\frac{\Delta(V_1)}{B(V_1)}\right] > 0. \tag{9}$$

In fact, (9) represents a necessary condition for existence of the equilibrium velocity $V_E$ (c.f. Fig. 5) for the crack zone configuration of Fig. 7 (a). There is no need to examine the energy balance of the propagation process, it is always satisfied for any equilibrium configuration of the crack zone because the displacements were found from an elastic solution and the singularities were abolished [12].

In this work, the validity of inequality [9] will be assumed. The present model makes it possible to evaluate $\Delta V$ but the kinematics of crack zone motion must be analyzed first [14].

Penetration of microcracks will be completed when the crack zone attains the configuration of Fig. 7 (b). As in the former case, a steady state motion of the zone will be assumed just prior to arrest of easy cleavage. The acceleration of point $A$ to $V_A = V_2$ will not be felt at $C$ and the equilibrium length of the zone, $s_{02}$, will be that corresponding to $V_A = V_1$. The equilibrium configuration of Fig. 7 (b) can be found from the finiteness condition, which is

$$P\sqrt{(a)} + \frac{\pi}{4}(\sigma_P - \sigma_0)\sqrt{(s_1)} - \sigma_P\sqrt{(s_{02})} = 0 \tag{10}$$

and from the condition that the crack opening displacement between $B$ and $C$ must not induce plastic strains. When $v_B$ denotes the limiting value, the displacement at $B$ is:

$$\frac{V_B}{B(V_1)} = \sqrt{(s_1')}\left[P\sqrt{(a)} - \sigma_P\sqrt{(s_{02})}\left(1 - \frac{2}{3}\frac{s_1}{s_{02}}\right)\right]. \tag{11}$$

In derivation of equation (10), the stresses transmitted by the links for $-s_1 < x < 0$ were assumed to follow the elastic distribution:

$$\sigma_{yy|x=0} \approx \frac{1}{\pi}\sigma_P \tan^{-1}\left[\frac{2\sqrt{(s(x+s_1))}}{x + s_1 - s}\right].$$

Equations (10) and (11) represent a system with two unknowns $s_1$ and $s_{02}$. It can be shown that there is only one real solution of this system. When only terms of the same order of magnitude are retained and for $v_B \to 0$ (Fig. 4), the solution is

$$s_1 = \left[1{\cdot}179\,\frac{\sigma_P - \sigma_0}{\sigma_P}\right]^2 s_{02}$$

$$s_{02} = \frac{P^2 a}{\sigma_P^2}\left[\frac{1}{1 - 0{\cdot}925\left(\frac{\sigma_P - \sigma_0}{\sigma_P}\right)^2}\right]^2. \qquad (12)$$

Graphical representation of those results is given in Fig. 9 which shows also the solution $s_0$ of equation (5). The lengths of crack zones are velocity independent because they were found from a steady state approximation.

The results of Fig. 9 may be related to any given crack geometry through Irwin's stress intensity factor [15, 16]

$$K_I = \frac{2\sqrt{2}}{\pi} P\sqrt{a}.$$

The time $t_p < t_2$ required for penetration of easy cleavage may now be evaluated (Fig. 7, 8)

$$t_p = \frac{s_{02} - s_0}{V_C - V_1} \qquad (13)$$

while

$$t_2 = \frac{2 s_0 c_2}{(V_1 + c_2)(c_2 - V_C)}. \qquad (14)$$

The transition between $t_p < t_2$ and $t_p > t_2$ will depend on the velocity $V_1$ and on the ratio $s_{02}/s_0$. In particular, for $t_p = t_2$,

$$\frac{s_{02}}{s_0} = \frac{2\,c_2(V_C - V_1)}{(V_1 + c_2)(c_2 - V_C)} + 1.$$

This relationship is plotted in Fig. 10 for variable ratios of $V_1/c_2$ and $V_C/c_2$ (solid lines). As the velocity $V_1$ increases from $V_1 = 0$ to $V_1 = V_C$, the value of $t_p$ also increases and for any grain size there is a value of $V_1$ such that $t_p > t_2$ for $V_A > V_1$. Since the ratio of the respective crack zone lengths depends only on the grain size and on the surface energy $\gamma$, the transition in the motion mode may be also related to grain size. The dashed lines in Fig. 10 represent the ratio $s_{02}/s_0$ as a function





of grain size $d^{-1/2}$. This ratio increases with decreasing $\gamma$. Hence, when $\gamma$ is low, transition to $t_p > t_2$ will occur at lower values of $V_1$ and in finer grain sizes. For example, if $\gamma = 5000$ ergs/cm$^2$, $V_C/c_2 \approx 0{\cdot}6$ and $d^{-1/2} \sim 6$, the transition will occur at $V_1 = 0{\cdot}2\ c_2$.

The remaining parameters of crack motion for $t_p < t_2$ may be evaluated from Fig. 8.

**Motion with interference, $t_p > t_2$**

The difference between this and the former motion mode will be reflected in evaluation of the velocity $V_2$ of point $A$ at arrest of the cleavage front. Because the acceleration of $A$ will be felt at $C$ before cleavage is arrested, we will assume that a quasi-steady state configuration of the zone will develop. The velocity of propagation of the equilibrium crack configuration, $V_2$, will be considered as the average velocity of point $A$ between $t = t_1$ and $t = t_4$, Fig. 8. Hence, as in the former case, the finiteness condition [10] will be valid and so will be the displacement relationship [11], when $s_{02}$ is replaced by $s_3$. In addition, the displacement at point $A$ will be:

$$\frac{v_A}{B(V_2)} = \frac{\epsilon_c \Delta(V_2)}{B(V_2)} = \sqrt{(s_3)}\left[P\sqrt{(a)} + (\sigma_P - \sigma_0)\sqrt{(s_1)}\left(1 - \frac{\pi}{4} + \frac{1}{4}\frac{s_3}{s_1}\right)\right]. \qquad (15)$$

From equations (10) and (11), $s_3 = s_{02}$, and results obtained in the previous paragraph apply. The velocity $V_2$ can be obtained directly from equation (15). In particular, when the inequality [9] is valid, $V_2 > V_1$. When both velocities $V_1$ and $V_2$ are known, the time period of crack motion can be found from Fig. 8.

**Discussion**

There are several experimental investigations which support individual aspects of the present model. In particular, the early work of Tipper [17] indicates the existence of step-like markings on the fracture surface and includes one of the first suggestions that microcracks spread ahead of the main crack. More recently, Pratt and Stock [18, 19] had studied the microstructural aspects of crack propagation. They found twins responsible for crack nucleation and it appeared difficult to locate isolated microcracks even ahead of arrested secondary cracks. This is in agreement with an earlier observation by Tipper and by Boyd [20]. Such results tend to confirm the basic premise of the proposed model that microcracks propagate in a continuous manner ahead of the main crack.

While the present work does not explain formation of the chevron pattern, it indicates that roughness of the fracture surface will increase with crack velocity. As crack zones will tend to move with interference,

the step length will increase and also, the thickness of the randomly penetrated and plastically deformed fracture surface layer is an increasing function of velocity [14]. Indeed, low velocity fractures are markedly smooth with no traces of chevrons.

Direct observation of the stepwise crack propagation process was made by van Elst and Veerbraak by means of high-speed photography and by Carlsson [10, 21]. There is always some uncertainty about the reliability of such experiments because of the shear lip formation at the observed surface, but perhaps this is less significant at lower temperatures. Let us consider one of such measurements performed at −35 °C, i.e., about 60°C below the crack arrest temperature. The material was low carbon steel of approximate grain size ASTM 7, $d^{-1/2} = 6$ mm$^{-1/2}$. At a location where $P\sqrt{(a)} \approx 25{,}000$ psi $\sqrt{(\text{in})}$ the average crack velocity was $V = 1{\cdot}5$ mm/$\mu$sec, the maximum observed length of a cleavage step was 2 mm and the maximum halting time of the cleavage front was 1 $\mu$sec. From Fig. 8, when the velocities $V_1$ and $V_2$ are replaced by an average $V$, the step length is equal to $V_C\ t_p$, while the halting time is $t_s - t_p$. Taking $\gamma = 10{,}000$ ergs/cm$^2$ and $V_C = 0{\cdot}6\ c_2$, we obtain from (13) and Figs. 8 and 9, the step length as 2·1 mm and the halting time 0·32 $\mu$sec. The predicted step length is also in good agreement with that reported by Tipper [17]. The discrepancy between the measured and predicted halting times is to be expected. The normal to the cleavage front at the plate surface will probably contain a large angle with that at the center of the plate. Hence, large velocities of easy cleavage and large halting times will appear in surface observation.

The actual photographs clearly reveal periodically developing steps of material weakening ahead of the main crack. There is, however, an appreciable variation in length of individual steps. This is due to the irregularity of the cleavage front which is predicted by the present model [1].

**Acknowledgement**

The author wishes to acknowledge gratefully the continuous and stimulating attention of Professor D. C. Drucker to this work. Financial support was provided by the Advanced Research Projects Agency through Contract SD-86 with Brown University and later by the Department of Civil Engineering at Duke University.

**References**

1. DVORAK, J. 'A model of brittle fracture propagation'. To appear in Engineering Fracture Mechanics.
2. HAHN, G. T., AVERBACH, B. L., OWEN, W. S. and COHEN, M. 'Initiation of cleavage microcracks in polycrystalline iron and steel' in *Fracture*, John Wiley, New York, 1959, pp. 91-116.





3. COHEN, M. 'Metallurgical structure and the brittle behavior of steel'. Ship Structure Committee, SSC-183, 1968.
4. HULL, D. 'Effect of grain size and temperature on slip, twinning and fracture in 3% silicon iron'. *Acta Met.*, vol. 9, p. 191, 1961
5. DRUCKER, D. C. 'Macroscopic fundamentals in brittle fracture'. Division of Engineering, Brown University Rept. AEC No. AT(30-1) 2394/27, 1967. To appear in *Treatise on Fracture*, ed. by H. Liebowitz, Academic Press.
6. SCHARDIN, H. 'Velocity effects in fracture' in *Fracture*, ed. by Averbach, B. L., Felbeck, D. K., Hahn, G. T. and Thomas, D. A., John Wiley, New York, 1959, pp. 297-329.
7. BARTON, F. W. and HALL, W. J. 'Brittle fracture tests of six-foot wide prestressed steel plates'. *Welding Joumal*, vol. 39, *Res. Suppl.*, p. 379s, 1960.
8. ERDOGAN, F. 'Crack propagation theories' NASA CR-901, Washington, D.C., 1967.
9. IRWIN, G. R., KRAFFT, J. M., PARIS, P. C. and WELLS, A. A. 'Basic aspects of crack growth and fracture', NRL Rept. 6598, 1967.
10. ELST, H. C. van 'The intermittent propagation of brittle fracture in steel'. *Trans. AIME*, vol. 230, p. 460, 1964.
11. CRAGGS, J. W. 'On the propagation of a crack in an elastic-brittle material'. *J. Mech. Phys. Solids*, vol. 8, p. 66, 1960.
12. MUSKHELISHVILI, N. I. 'Some basic problems of the mathematical theory of elasticity', 5th Russian edition, Nauka, Moscow 1966.
13. GOODIER, J. N. and FIELD, F. A. 'Plastic energy dissipation in crack propagation' in *Fracture of Solids*, ed. by D. C. Drucker and J. J. Gilman, Interscience, New York, 1962, pp. 103-118.
14. DVORAK, J. To be published.
15. PARIS, P. C. and SIH, G. C. 'Stress analysis of cracks'. in *Fracture toughness testing and its applications*, ASTM STP 381, Philadelphia, 1964, pp. 30-81.
16. RICE, J. R. 'Plastic yielding at a crack tip' Proc. Int. Conf. Fracture, Sendai. P. Noordhoff, 1965.
17. TIPPER, C. F. 'The study of fracture surface markings'. *J. Iron Steel Inst.*, vol. 179, p. 4, 1957.
18. PRATT, P. L. and STOCK, T. A. C. 'The distribution of strain about a running crack', *Proc. Roy. Soc.* London, vol. 285A, p. 73, 1965.
19. STOCK, T. A. C. and PRATT, P. L. 'Microstructural damage adjacent to a brittle fracture', *Brit. Weld. Jnl.*, p. 631, 1966.
20. BOYD, G. M. 'The conditions for unstable rupturing of a wide plate', *Trans. Inst. Naval Archit.*, vol. 99, p. 349, 1967.

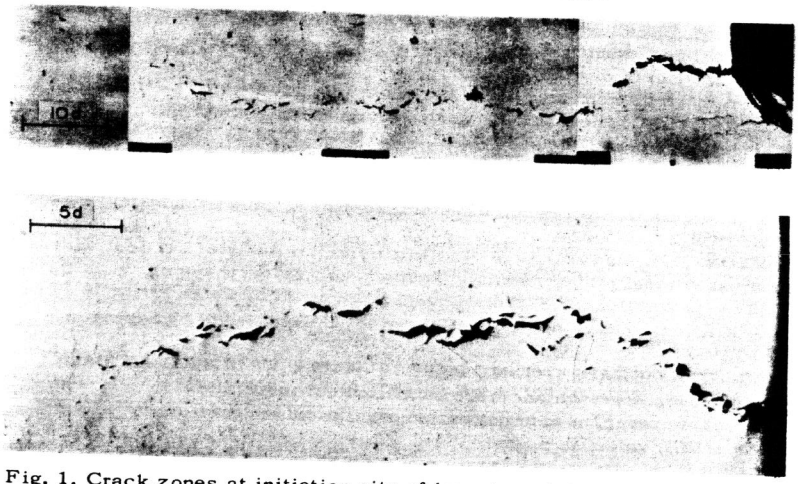


Fig. 1. Crack zones at initiation site of low-stress brittle fracture in mild steel. × 50.

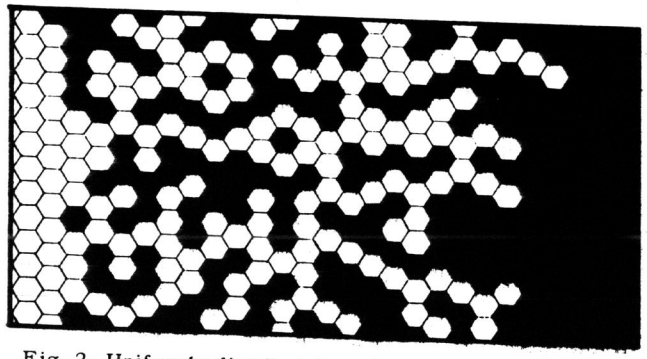

Fig. 2. Uniformly distributed weakening of about one half of all grains by easy cleavage in the crack zone.





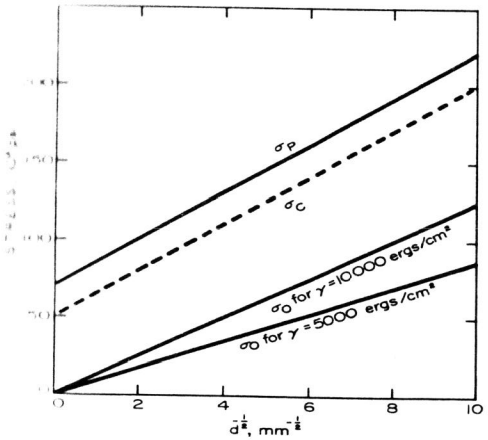


Fig. 3. Stresses in the crack zone as functions of grain size *d*. All values are related to the original crossection.

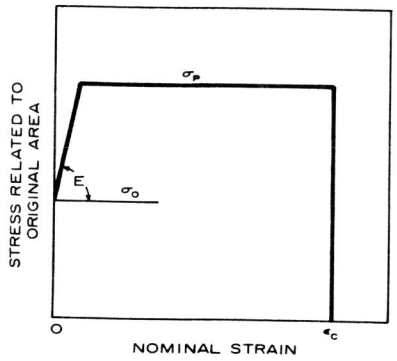


Fig. 4. Mechanical properties of the links in the crack zone.

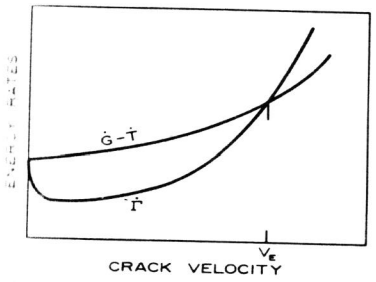


Fig. 5. The equilibrium velocity of a brittle crack. *G* is the strain energy, *T* is the kinetic energy and $\Gamma$ is the surface energy.

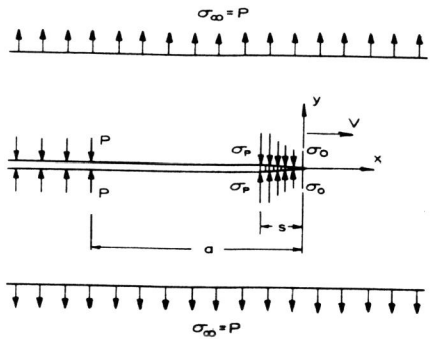


Fig. 6. The steady state crack.

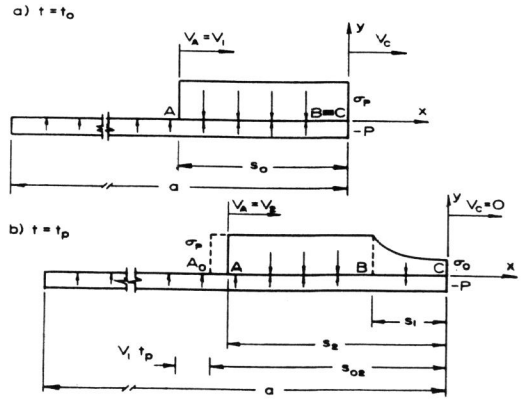


Fig. 7. Configurations of the crack zone. (a) at onset of easy cleavage, (b) when easy cleavage penetration is completed.

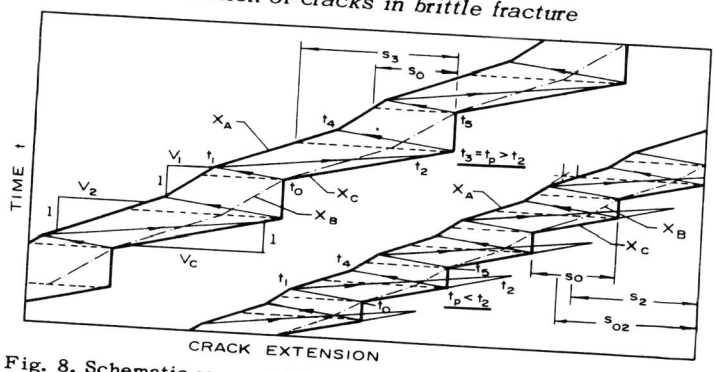


Fig. 8. Schematic representation of motion of the crack zone for the two basic modes, $t_p > t_2$ and $t_p < t_2$.

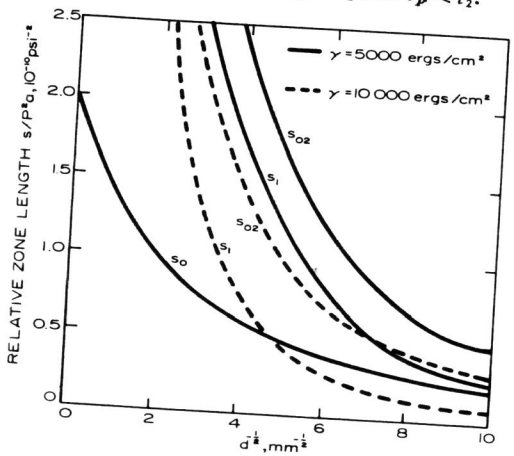


Fig. 9. Equilibrium lengths of crack zones.

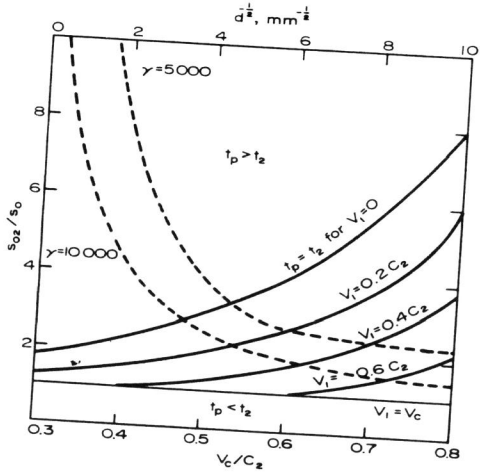


Fig. 10. Transition in crack zone motion mode. (The lower scale is for solid lines, the upper scale is for dashed lines.)